Vol. 09, No. 01 (2025) 43 – 55
JIIF (Jurnal Ilmu dan Inovasi Fisika)
https://jurnal.unpad.ac.id/jiif/

THE EFFECT OF CALCINATION TEMPERATURE ON ZnO CRYSTALS BASED ON EMISSION SPECTRUM FROM PHOTOLUMINESCENCE CHARACTERIZATION

J ASKARIYYA[1], A APRILIA[2]*, N RIVELI[2], L SAFRIANI[2], FITRILAWATI[2]

[1]*Bachelor of Physics Study Program, Faculty Mathematics and Natural Sciences, Universitas Padjadjaran,*
[2]*Physics Department Faculty Mathematics and Natural Sciences, Universitas Padjadjaran,*
Jl. Raya Bandung-Sumedang km 21 Jatinangor, Sumedang, Jawa Barat, Indonesia

**Corresponding author*
Email: a.aprilia@phys.unpad.ac.id

Diserahkan: 07/01/2025
Diterima: 21/01/2025
Dipublikasikan: 06/02/2025

Abstract. ZnO is a semiconducting material widely used in optoelectronic devices, such as gas sensors, photocatalysts, and solar cell photoanodes. ZnO's electrical and optical properties are strongly related to particle size, crystal quality, and defect states, which in turn depend on the preparation process, including the synthesis method and calcination temperature. This study synthesized ZnO powder using the sol-gel method to investigate its optical properties. ZnO samples were calcined at 150°C, 300°C, and 450°C under a nitrogen (N_2) flow. TGA/DTA analysis showed that most solvent residues and impurities were decomposed at 450°C. This result is supported by XRD analysis, which showed increased crystallinity with rising temperature. At the same time, the hexagonal wurtzite structure of the ZnO gel remained intact after calcination. SEM-EDS analysis revealed an agglomerated morphology and a disproportionate Zn:O ratio in all samples, with excess Zn atoms, likely due to interstitial Zn defects. The photoluminescence spectrum showed higher intensity in the UV region compared to the visible range, indicating good crystallinity. The blue shift in the emission with increasing temperature indicates the presence of several different defects in the material. In particular, the green emission associated with oxygen vacancies was absent in the sample calcined at 450°C. This result confirms that higher calcination temperatures reduce defects and increase crystallinity. Based on these findings, lower calcination temperatures produce smaller crystal sizes, suitable for nano-optical applications, such as photocatalysis, due to oxygen vacancies.

Keywords: ZnO, Crystal, calcination, photoluminescence, defect

Abstrak. *ZnO adalah material semikonduktor yang banyak digunakan dalam perangkat optoelektronik, seperti sensor gas, fotokatalis, dan photoanoda sel surya. Sifat listrik dan optik ZnO sangat terkait dengan ukuran partikel, kualitas kristal, dan keadaan cacat, yang pada gilirannya bergantung pada proses persiapan, termasuk metode sintesis dan suhu kalsinasi. Dalam penelitian ini, bubuk ZnO disintesis menggunakan metode sol-gel untuk menyelidiki sifat optiknya. Sampel ZnO dikalsinasi pada suhu 150°C, 300°C, dan 450°C di bawah aliran nitrogen (N_2). Analisis TGA/DTA menunjukkan bahwa sebagian besar sisa pelarut dan kotoran terurai pada suhu 450°C. Hasil ini didukung oleh analisis XRD, yang menunjukkan peningkatan kristalinitas seiring dengan meningkatnya suhu. Pada saat yang sama, struktur wurtzite heksagonal dari gel ZnO tetap utuh setelah kalsinasi. Analisis SEM-EDS mengungkapkan morfologi yang teragregasi dan rasio Zn:O yang tidak seimbang pada semua sampel, dengan atom Zn berlebih, yang kemungkinan disebabkan oleh cacat Zn interstisial. Spektrum fotoluminesensi menunjukkan intensitas yang lebih tinggi di wilayah UV dibandingkan dengan rentang tampak, yang mengindikasikan kristalinitas yang baik. Pergeseran biru pada emisi*

DOI: https://doi.org/10.24198/jiif.v9i1.60621 *e-ISSN: 2549-7014*

seiring dengan meningkatnya suhu menunjukkan adanya beberapa cacat yang berbeda dalam material tersebut. Secara khusus, emisi hijau yang terkait dengan kekosongan oksigen tidak terdeteksi pada sampel yang dikalsinasi pada suhu 450°C. Hasil ini mengonfirmasi bahwa suhu kalsinasi yang lebih tinggi mengurangi cacat dan meningkatkan kristalinitas. Berdasarkan temuan ini, suhu kalsinasi yang lebih rendah menghasilkan ukuran kristal yang lebih kecil, yang cocok untuk aplikasi nano-optik, seperti fotokatalisis, karena adanya kekosongan oksigen.

Kata kunci: ZnO, kristal, proses kalsinasi, fotoluminesensi, cacat kristal.

1. Introduction

Zinc Oxide (ZnO) is one of the semiconductor materials widely studied by the scientific community since the 1930s. Various studies discovered several characteristics of ZnO, such as its crystal lattice parameters and optical properties [1]. Recently, ZnO has been developed into various forms, such as bulk, thin films, and nano-sized powders, and is commonly used as active material in photocatalysts, electronic devices, etc. [2]. The development resulted in a wide range of ZnO nanostructures, such as nanorods, nanowires, nanoflowers, and nanoparticles. Recently, research interest in ZnO nanostructures has been growing massively due to this type of oxide semiconductor's unique properties and wide applications [3].

ZnO is one of the functional materials with good physical and chemical properties. It has strong chemical stability, a wide radiation absorption spectrum, and high photostability. ZnO is a semiconductor material associated with group II-VI with a band gap energy of approximately 3.37 eV and an exciton binding energy of 60 meV [1]. This anti-bacterial material has non-toxic properties, so it does not trigger diseases such as cancer and is not harmful to human reproduction [4, 5]. Three (3) types of ZnO crystal structures are cubic zinc blende, cubic rock-salt, and hexagonal wurtzite. At atmospheric pressure and room temperature, ZnO is usually obtained in a hexagonal wurtzite structure with lattice parameter values *a* and *c* of 0.3296 nm and 0.5206 nm [6]. Our previous study showed that the ZnO crystal structure had formed at a low heating temperature of 150 ℃ [7]. ZnO has high optical transmission in the visible region, making it a preferable candidate for optoelectronic applications, such as LEDs, laser diodes, photovoltaic devices, solar cells, and so on [8]. Its ability to absorb some radiation in the UVA (320-400 nm) and UVB (290-320 nm) ranges also makes this material desirable in beauty fields, such as sunscreen [5,9]. However, defects in ZnO can play a significant role in its optical properties and influence its performance in certain applications [8].

Defects in materials can be observed through photoluminescence (PL) characterization. Two emission spectrum types are usually found in ZnO PL spectra; one is centered in the UV region, and the other is in the visible region. The emission spectrum in the UV region correlates to the recombination of electrons located in the conduction band with holes in the valence band. On the other hand, the presence of emissions in the visible region is usually considered as the existence of crystal defects, such as zinc interstitials (Zn_i), oxygen vacancies (V_o), zinc vacancies (V_{Zn}), and other types of defects [10]. Shaymardanov et al. observed the changes in ZnO crystal defects identified from the heated material's PL spectra at different temperatures [11]. It was also found that ZnO synthesized using the chemical bath deposition method showed a shift in green emissions towards lower wavelengths (blueshift) after calcined at high temperatures under the N_2 atmosphere. These green emissions that relate to the existence of oxygen vacancy affect the photocatalytic activity [11]. On the other hand, based on our previous study, ZnO

synthesized using the sol-gel method showed a blue emission peak in samples calcined at high temperatures in the air atmosphere [7].

The peak in its PL spectra also showed a blueshift in the blue emission region as the calcination temperature increased. However, the defects that appear in this blue emission slow down the rate of pollutant degradation [7]. Shen et al. (2022) also reported that using different excitation lambda can obtain a specific PL emission spectrum pattern [12]. This can also provide complete/comprehensive information about which defects existed in the sample. The calculation was carried out in different atmospheres, such as the N_2 atmosphere, which aims to prevent unwanted reactions [12]. Based on several results from researchers, the heating conditions (temperature and air) can affect certain defects identified in the material. Therefore, in this study, ZnO materials were calcinated at 150°C, 300°C, and 450°C in the N_2 atmosphere. This research is conducted to determine the effects of calcination temperature on crystal structure defects identified through PL characterization of ZnO.

2. Research Methods

ZnO nanoparticles in powder form were synthesized using the sol-gel method. One gr of Zinc Acetate Dehydrate ($Zn(CH_3COOH)_2 \cdot 2H_2O$) as precursor dissolved in 42 ml of methanol. The solution was placed in the three-neck bottle, and the condenser was set up and stirred at a temperature of 65°C using a magnetic stirrer. While the solution was stirred, the catalyst solution was prepared by mixing 0.28 gr of NaOH and 23 ml of methanol using an ultrasonic bath for 15 minutes at room temperature (±27°C). This catalyst solution was then dropped wisely into the precursor solution. The stirring continued until the solution color changed to cloudy white, indicating a hydrolysis reaction in the material. After about an hour of stirring, the color solution returned from cloudy white to transparent, which indicated a condensation reaction of the solution. About 90 minutes afterward, the solution undergoes a second color change from transparent to milky white. This confirms that the phase changes from solution to gel and that the stirring process is finished. The solution can be put into a bottle and left for 2 days until precipitate occurs (aging). The precipitation was collected and washed using n-hexane and methanol in a ratio of 1:1. To separate the ZnO gel precursor from the residue and solvent, the solutions were centrifuged for 10 minutes at 3600 rpm. The process was carried out up to 3 times, and ZnO was obtained as a dry gel. The synthesis process can be repeated if the sample does not form a proper precipitate after this washing process. The drying process was performed using a vacuum oven, where the ZnO dry gel was vacuumed for 12 hours and heated afterward for 8 hours at 150°C. The ZnO granules were crushed into a powder using a mortar. The ZnO powders obtained were treated post-calcination using a tube furnace with N_2 flow at 150°C, 300°C, and 450°C. Each sample were identified as ZnO-15, ZnO-15 (N_2), ZnO-30 (N_2), and ZnO-45 (N_2).

The crystal structure of ZnO powder was analyzed using an X-ray diffractometer (XRD) Bruker D8 Advance. This characterization was performed for ZnO dry gel (as prepared), ZnO-15, ZnO-30 (N_2), and ZnO-45 (N_2). The results obtained are intensity versus diffraction angles curves, which are matched with references from the crystallographic open database (COD). TGA/DTA (thermogravimetry analysis/differential thermal analysis) characterization was performed on Hitachi STA 7300 to investigate thermal properties and study the changes of ZnO dry gel becoming ZnO crystal. During the process, ZnO-dry gel was placed in an inert atmosphere with a nitrogen (N_2) gas flow and heated from room temperature up to 1000°C, gradually rising to 10°C/minute. To support

TGA/DTA data, Fourier Transform Infrared (FTIR) characterization was carried out. The spectrum obtained was then compared with existing references to investigate any certain chemical bonds in ZnO dry gel. SEM/EDS was carried out using an SU3500 electron microscope to determine morphology and composition. UV-visible and Photoluminescence (PL) spectroscopy were performed to analyze the optical properties of ZnO powders that resulted in different calcination conditions. The UV-Vis spectra with 200-500 nm wavelengths were performed on a TG70+ UV/VIS Spectrometer. The data obtained from this spectroscopy can be processed to determine band-gap value using the Tauc-Plot method. On the other hand, emission spectra were analyzed through Perkin Elmer LS-55 Fluorescence Spectrometer utilising the variation of excitation wavelengths of 275 nm, 300 nm, 325 nm, and 350 nm. The spectrum's deconvolution was performed using Gaussian distribution to identify each curve's position. The peak locations of each deconvoluted curve were obtained and analyzed.

3. Results and Discussion

3.1 The inluences of heating temperature to the ZnO Crystal Structure

The crystal structure of ZnO-dry gel (as prepared), ZnO-15, ZnO-30 (N_2), and ZnO-45 (N_2) were investigated from XRD patterns that are shown in Figure 1.

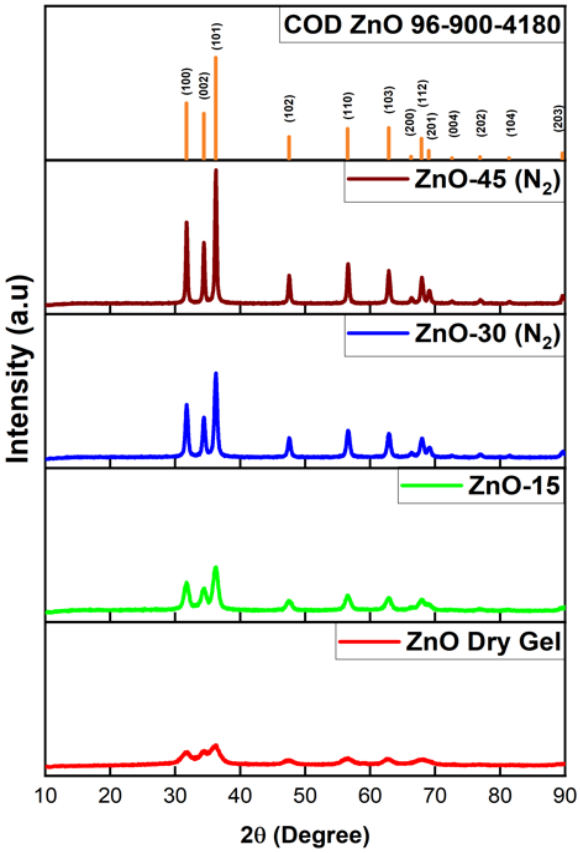

Figure 1. XRD graphs of ZnO Dry Gel, ZnO-15, ZnO-30 (N_2), ZnO-45 (N_2) samples compared with the reference

These peaks were compared with the COD No. 96-900-4180. All samples show patterns that match the ZnO hexagonal wurtzite structure. The XRD patterns of ZnO dry gel have the lowest intensity compared to the other samples. In Table. 1, calculation

results of lattice parameters and sample cell volumes are tabulated. The lattice parameter calculation was carried out using equation (1). This calculation resulting the value of $a=b\neq c$, which also confirmed the lattice parameter values of the hexagonal structure.

$$\frac{1}{d_{hkl}^2} = \left[\frac{4}{3}(h^2 + hk + k^2) + l^2\left(\frac{a}{c}\right)^2\right]\frac{1}{a^2} \quad (1)$$

where *d* is atomic spacing, and *hkl* is the Miller index. Based on these results, it is known that heating temperature does not change the crystal structure of the samples but changes the size of the crystalline grains, as shown in Table 1.

Table 1. Comparison of lattice parameters, crystallite size, DoC and Cell Volume of samples with COD reference

Material	*a=b* (Å)	*c* (Å)	FWHM	Crystallite Size (*D*) nm	Volume Cell (Å^3)	DoC (%)	δ (×10^{-5} nm^{-2})
COD 96-900-4180	3.253	5.207	-	-	47.72	-	-
ZnO-Dry Gel	3.258	5.218	2.37	5.34	47.96	49.9	0.035
ZnO-15	3.253	5.213	1.01	9.29	47.77	63.4	0.011
ZnO-30 (N_2)	3.251	5.208	0.56	16.79	47.67	72.7	0.003
ZnO-45 (N_2)	3.252	5.207	0.33	28.19	47.63	80.6	0.001

The intensity of the peaks increased with the temperature, followed by a decreasing value of Full Width Half Maximum (FWHM), which indicates a better crystallinity of the samples. The increase in crystallinity percentage occurs since the atoms in samples receive high thermal energy, which helps atoms to move to the right location. Due to higher crystallinity in the lattice, the crystal's defects decrease [13].

Degree of Crystallinity (DoC) values were obtained by calculating the ratio of the area of the crystal phase (Ac) to the entire curve (summation of amorphous phase (Aa) and Ac) using equation (2). It is necessary to reduce the background noise that usually appears in the XRD raw curve to identify the amorphous and crystal phases. The results show that ZnO-45 (N2) powder has the highest percentage of DoC compared to other samples. The crystallite size of the samples was calculated using the Debye-Scherrer equation (equation (3)), where *D* is crystallite size, *K* is Scherrer constant (0.98), β is the FWHM, and θ is the peak position (degree). The higher annealing temperature caused a larger size of the crystallites [13]. Through the annealing process, the sample receives enough energy to facilitate the diffusion and recrystallization of elements or compounds that cause the merging of small grains into larger grains [14]. The dislocation density (δ), which shows the presence of crystal defects per unit area in one unit cell, is calculated using equation (4) [15]. The results are consistent with DoC values, where ZnO-45 (N2), which has the highest degree of crystallinity (80.6%), shows the smallest value of dislocation density (0.001 nm-2).

$$DOC\ (\%) = \frac{A_c}{A_a + A_c} \quad (2)$$

$$D = \frac{K\lambda}{\beta cos\ \theta} \quad (3)$$

3.2 Morphology and Element Composition Analysis

The scanning electron microscope and energy dispersive spectrum (SEM/EDS) characterization results show the morphology and element composition of the sample. The samples were first coated with gold (Au) for better image results provided by the apparatus. The imaging data of the samples is shown in Figure 2.

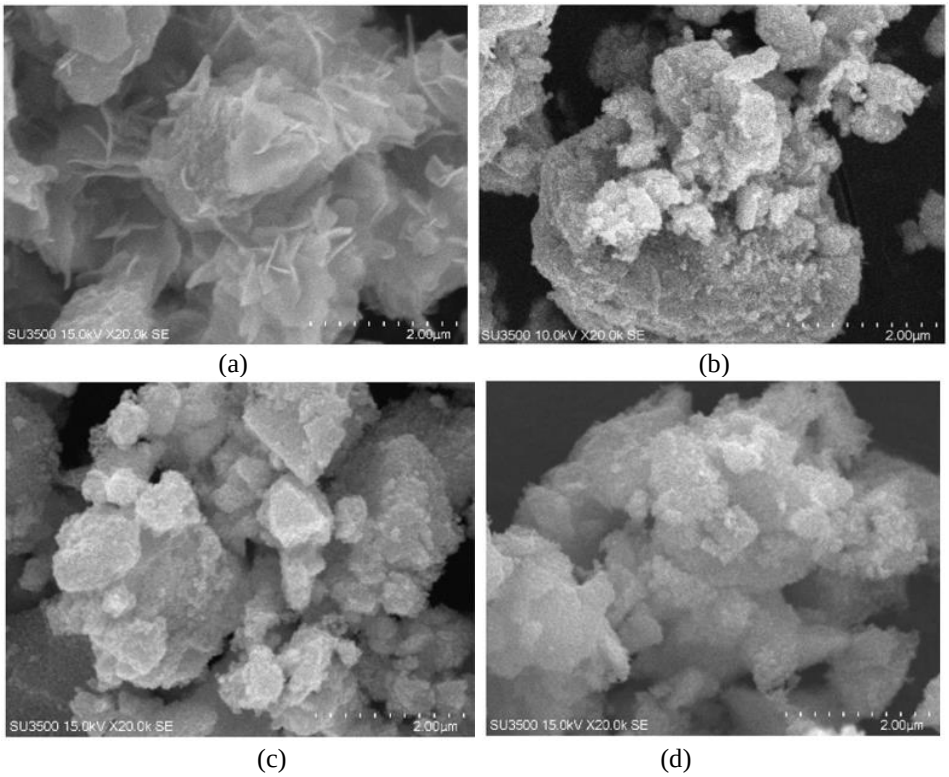

Figure 2. SEM results of samples (a) ZnO-15, (b) ZnO-15 (N_2), (c) ZnO-30 (N_2), (d) ZnO-45 (N_2)

The ZnO-15 shows an irregular shape and does not show a clear boundary between each particle. The agglomeration of particle grains likely causes this due to their surface energy, which eventually formed into a cluster [15, 16]. The grains are not entirely formed at a low calcination temperature, and the ions were assembled as small clusters [17]. Therefore, high energy is required to start crystal growth. On the other hand, in post-calcined samples, which are ZnO-15 (N_2), ZnO-30 (N_2), and ZnO-45 (N_2), the particle image shows an evenly distributed grain.

The EDS results are tabulated in Table 2. This data shows that all samples consist of two main elements, Zn and O. To numerically analyze this composition, the mass and atomic percentages of both elements are compared. It is known that the atomic ratio of Zn:O contained in all samples does not show an equal ratio (1:1), where the composition of Zn is greater than O. This may indicate that the samples have an excess of Zn element, which led to Zinc interstitial or oxygen vacancies defects [18]. It is known that using N_2 gas during calcination could cause the appearance of Zinc interstitial defects [19].

Table 2. Atomic composition of samples from EDS characterization

Material	Element	Mass (%)	Atomic (%)	Atomic Zn:O
ZnO-Dry Gel	Zn	87.23	62.57	1 : 0.59
	O	12.27	37.43	
ZnO-15	Zn	90.13	69.09	1 : 0.45
	O	9.87	30.91	
ZnO-30 (N_2)	Zn	86.65	61.37	1 : 0.63
	O	13.35	38.63	
ZnO-45 (N_2)	Zn	88.97	66.37	1 : 0.51
	O	11.03	33.63	

3.3 Interpretation of Thermal Analysis

The TGA curve shows the mass decomposition of the samples, while the DTA curve represents the occurrence of exothermic or endothermic reactions. Figure 3 shows the TGA/DTA measurement curve of ZnO dry gel. The TGA curve shows a 42% mass decrease in the temperature range of 22°C to 74°C. This represents a desorption of thermal energy to evaporate the water content, marked by the mass of the material significantly decreasing.

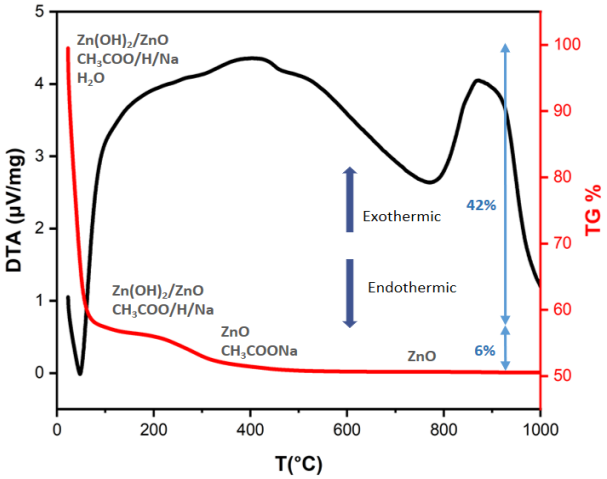

Figure 3. TGA-DTA graph of ZnO dry gel precursor

The evaporation of water molecules (H_2O) in ZnO dry gel contributed to this mass decrease. Along with this, the DTA curve shows an endothermic process in the temperature range in the temperature range of 22°C to 47°C, which is indicated by a strong peak formed. An endothermic process has a strong relationship with the absorption of heat energy by the samples. The FTIR characterization was performed to understand the ZnO crystal forming under the heating process and support the data interpretation. The FTIR spectra of ZnO dry gel and ZnO-15 are shown in Figure 4.

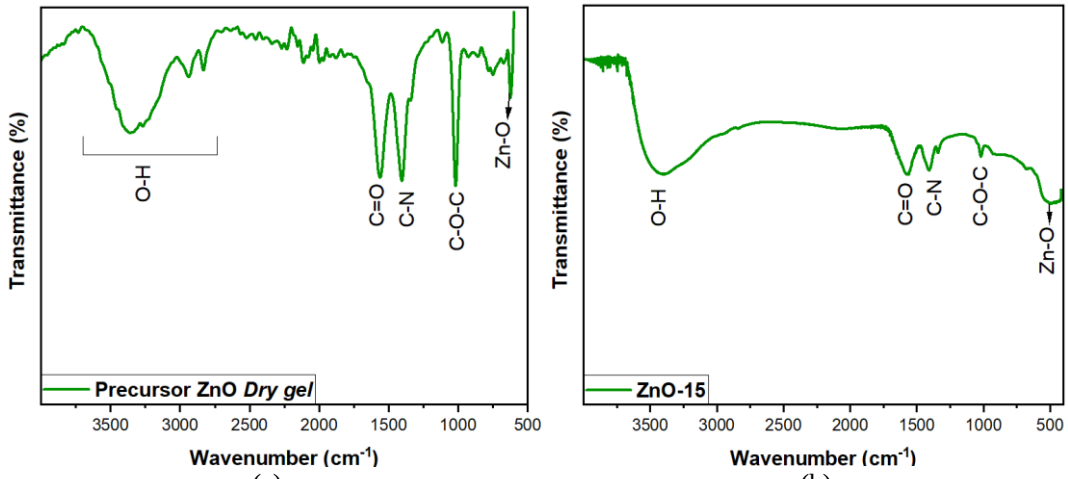

Figure 4. FTIR curves of (a) ZnO precursor dry gel, (b) ZnO-15

The ZnO bond has formed before and after being heated at 150°C. However, some other chemical bonds were still identified in the sample. This is also supported by the mass

decrease in the TGA curve that occurs under 150°C. About 6% of mass decrease occurs above 150°C, which is assumed to be the bond-breaking of $Zn(OH)_2$ to ZnO. The overall mass decrease based on the TGA characteristic curve in the sample is 48%. The DTA results show an exothermic reaction at a calcination temperature of 300°C, which correlated to the formation of ZnO crystals and the reduction of some hydrocarbon compounds. At a high temperature (450°C), the CH_3COONa bond and other hydrocarbon compounds started to break. From the DTA curve, an endothermic process occurs from 450°C to 775°C, decomposing residual reaction substances in the sample.

3.4 The Optical Analysis

UV-Vis (ultraviolet-visible) characterization was conducted with a range of 200 to 500 nm to investigate the optical properties from the absorption spectrum of the sample (Figure 5(a)). Photoluminescence spectroscopy (Figure 5(b)) was carried out with varying excitation wavelengths to study the correlation between ZnO preparation and the optical properties related to the defect state. The sample preparation was conducted by dispersing the powder samples of ZnO-15, ZnO-15 (N_2), ZnO-30 (N_2), and ZnO-45 (N_2) in methanol. The samples' absorbance peaks and emission spectrum can be observed through these two kinds of characterization.

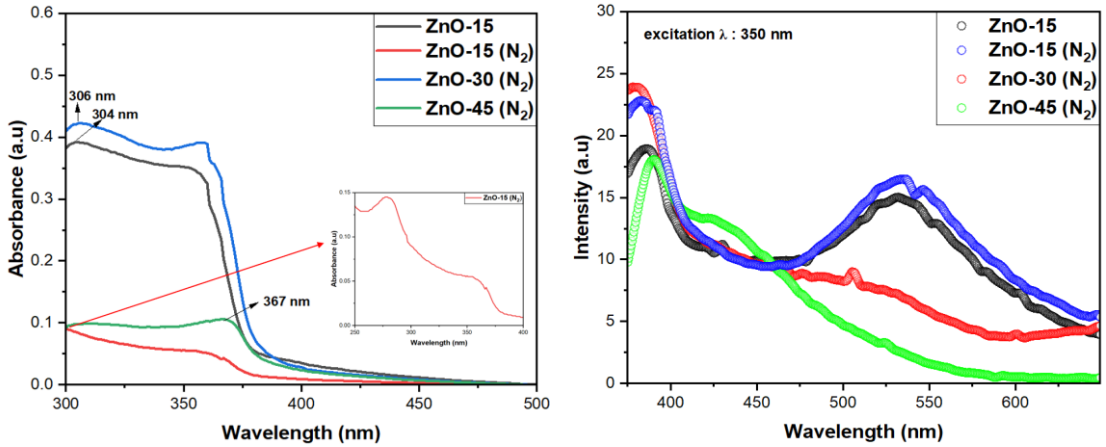

(a) (b)

Figure 5. (a) UV-Vis absorbance spectra from all sample, (b) PL curves using 350 nm excitation lambda of ZnO-15, ZnO-15(N_2), ZnO-30(N_2), ZnO-45(N_2) samples

It is known from Figure 5 (a) that all samples show a maximum absorbance spectrum below the wavelength of 400 nm. The difference in intensity in the samples is assumed to occur due to differences in particle size and density resulting from different heating conditions [20]. The λ_{ex} columns show a rounded value of wavelength where maximum absorbance occurs (Table 3).

Table 3. Maximum absorbance data of ZnO-15, ZnO-15 (N_2), ZnO-30 (N_2), ZnO-45 (N_2) samples

Sample	Maximum Absorbance (%)	λ_{ex} (nm)
ZnO-15	87.23	300
ZnO-15 (N_2)	12.27	275
ZnO-30 (N_2)	90.13	300
ZnO-45 (N_2)	9.87	350

This value will be used as a reference for PL excitation wavelength. The Tauc Plot method uses equation (5) to determine the band gap value of all samples. *A* is the Absorption

coefficient provided by the measurement, h is Planck's constant (6.63×10^{-34} J. s), ν is the Frequency of photon (Hz), E_g is the Band gap energy that calculates, and n is value of the type of transition that occurs.

$$(\alpha h\nu)^n = A(h\nu - E_g) \quad (5)$$

The Tauc Plot results are shown in Figure 6.

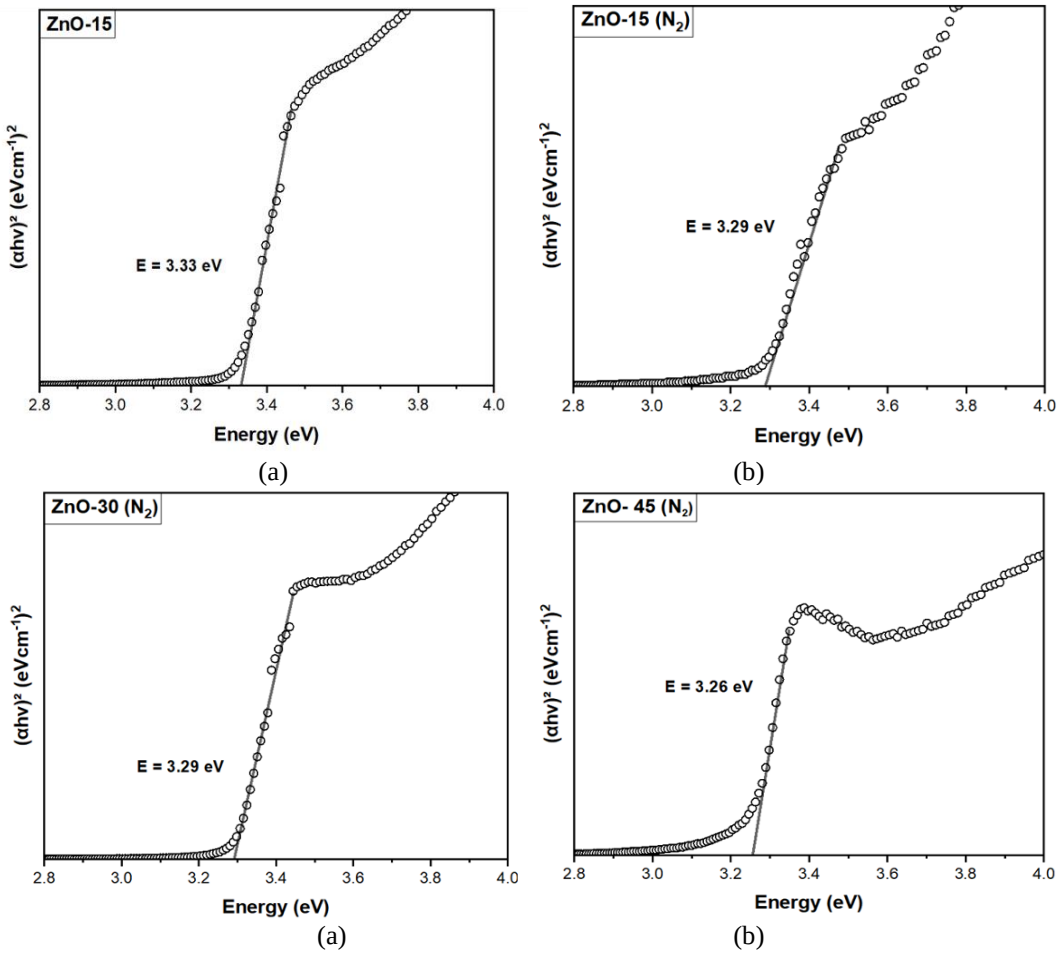

Figure 6. Band gap calculation using Tauc-plot method of (a) ZnO-15, (b) ZnO-15(N_2), (d) ZnO-30(N_2), and (c) ZnO-45(N_2)

It is known that ZnO-15, ZnO-15 (N_2), ZnO-30 (N_2), and ZnO-45 (N_2) have band gap values of 3.33 eV, 3.29 eV, 3.29 eV, and 3.26 eV, respectively. The band gap value decreases along with the increase of the calcination temperature used. This occurred due to the presence of shallow traps in the energy gap. It is also related to the increase in crystallite size and decrease in the amorphous phase in the material. Reducing sample defects is also likely to affect the decrease in band gap value [21].

Information about possible defects or impurities of ZnO can be obtained by analyzing the PL spectra of ZnO using different excitation wavelengths (λ_{ex}). Characterization was performed using four variations of λ_{ex} of 275 nm, 300 nm, 325 nm, and 350 nm. This excitation lambda value is based on the absorbance spectrum of all samples obtained from UV-Vis absorption chatarteristics. Based on the overall results of PL shown in Figure 7, it is known that there is a shift in the emission peak of all samples. In the analysis of PL results, the curve obtained using excitation lambda of 350 nm was observed further since

its energy value is closest to the literature band gap of ZnO (3.37 eV). This further observation was carried out by deconvolution using Gaussian distribution.

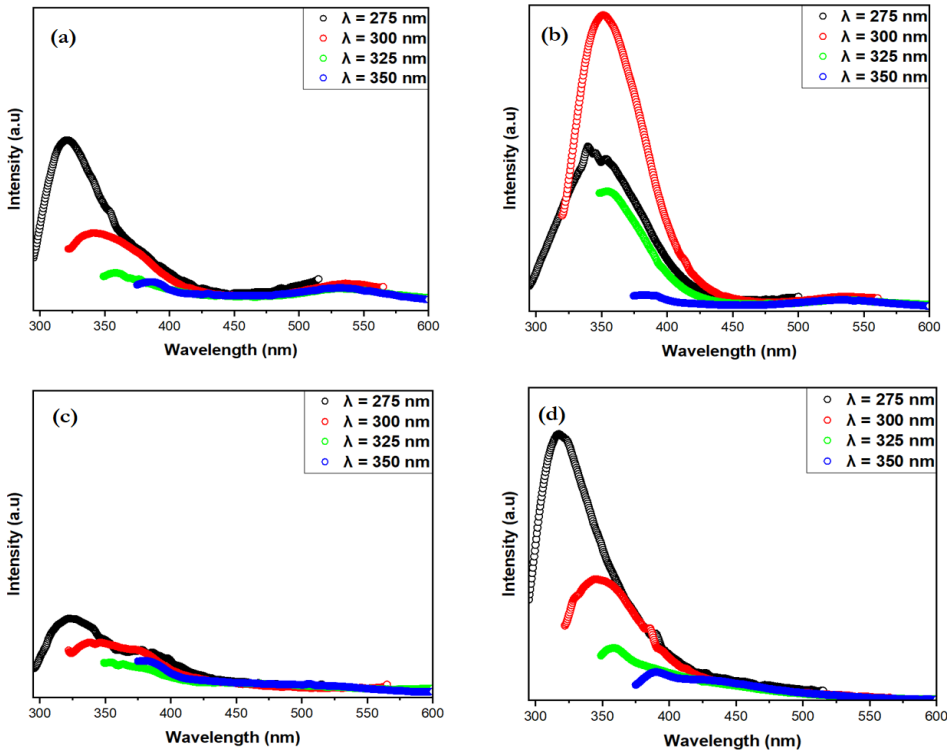

Figure 7. PL curves of samples (a) ZnO-15, (b) ZnO-15(N_2), (c) ZnO-30(N_2), (d) ZnO-45(N_2) using wavelengths of 275 nm, 300 nm, 325 nm, and 350 nm.

The deconvoluted curve of the sample presented in Figure 8 shows a high emission peak in the UV region and a low in the visible region, confirming good crystallinity in the sample. This is also supported by the value of the degree of crystallinity (DoC), as shown in Table 1, all of which have crystallinity above 50% for ZnO-15, ZnO-30 (N_2), and ZnO-45 (N_2) samples. The crystallinity of all samples increases with calcination temperature, followed by a reduction of defects in appearance in green emission. In all samples, there are similarities in identified emission patterns. Where the highest peak is always located in the UV region, and its peak intensity is reduced in the visible region. An emission in UV region is often associated with free exciton recombination (FX). Emissions in the visible range are most likely due to intrinsic defects in the material [12]. Common intrinsic defects formed in ZnO include zinc interstitials (Zn_i), oxygen vacancies (V_O), and zinc vacancies (V_{Zn}) [12]. This presence of local defects in a semiconductor is known to produce additional energy bands within the band gap region [17].

Another peak was also identified in the blue region of the ZnO-30 (N_2) sample at 452 nm and ZnO-45 (N_2) at 444 nm and 471 nm. This emission exists due to the emergence of zinc-interstitial defects that appear around 0.54 eV - 0.72 eV below the conduction band. N_2 gas flow during calcination can also correlate with Zinc interstitial defect, which relates to the environment's low oxygen levels. Green emissions appear in all ZnO-15, ZnO-15 (N_2), and ZnO-30 (N_2) samples at around 514 to 535 nm. This green emission peak shows a blueshift with increasing heating temperature, leading to its gradual reduction and eventual absence in the ZnO-45 (N_2) sample. The elimination of oxygen vacancy defects is confirmed after calcination at 450°C.

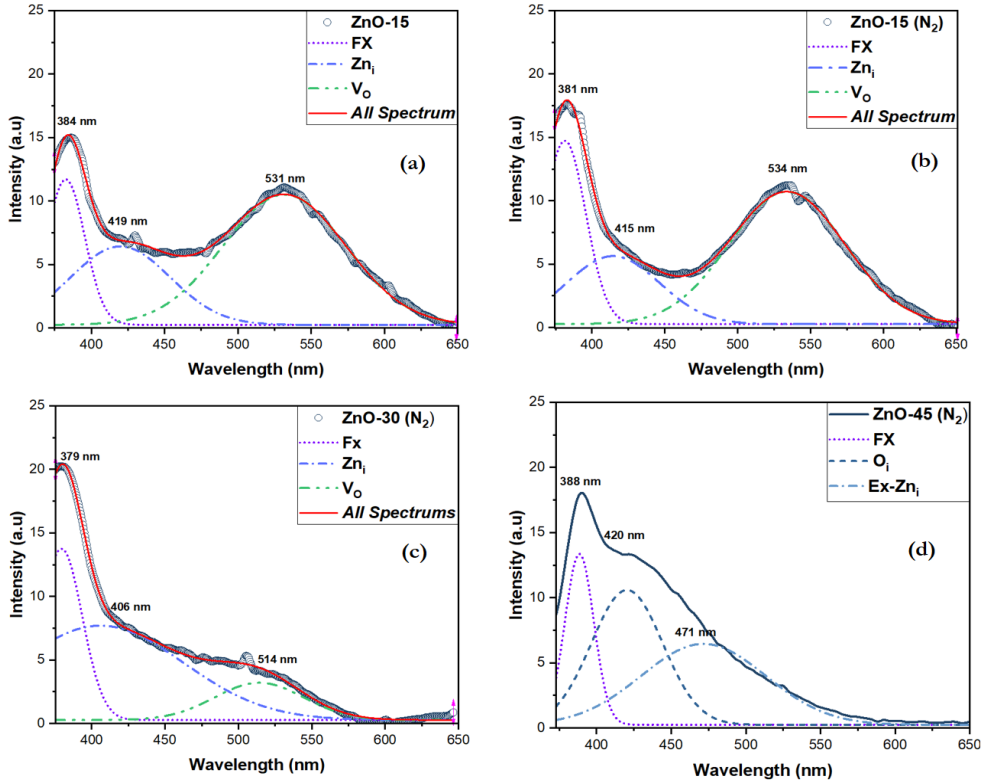

Figure 8. The results of the PL curve deconvolution of samples (a) ZnO-15, (b) ZnO-15 (N_2), (c) ZnO-30 (N_2), (d) ZnO-45 (N_2) using a wavelength of 350 nm.

Based on the deconvolution results of all four samples, the defect states that possibly appeared are illustrated in the energy level diagram shown in Figure 9.

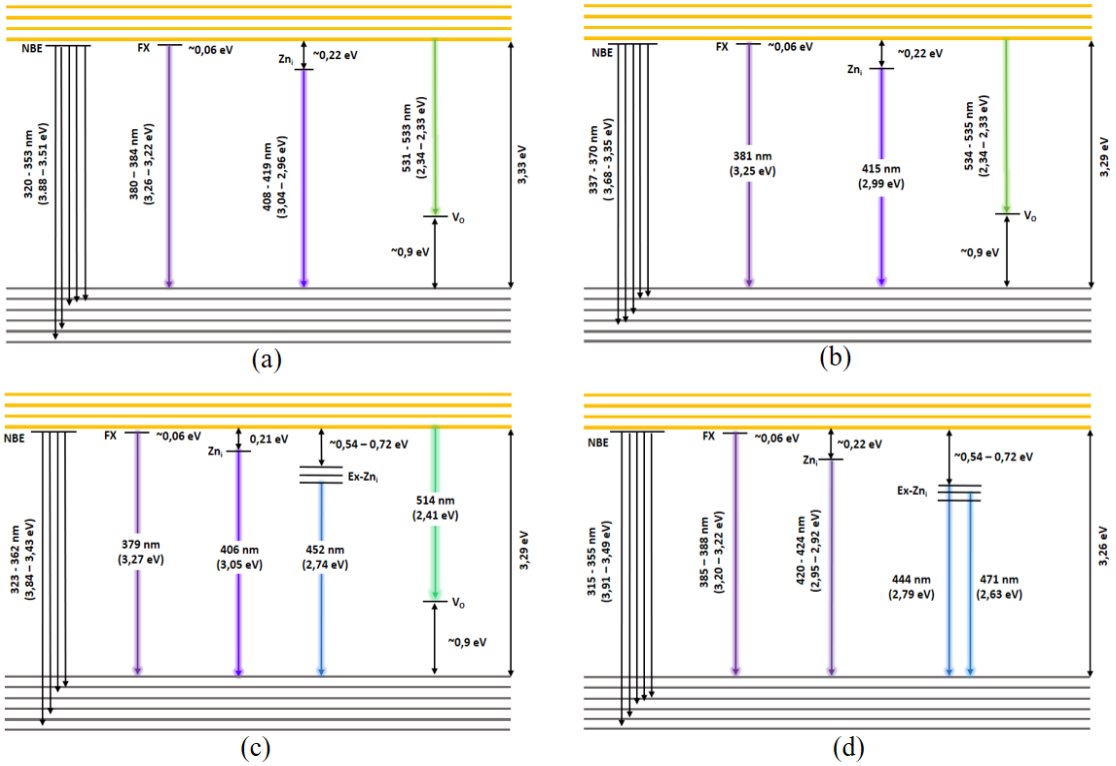

Figure 9. Defect energy levels in samples (a) ZnO-15, (b) ZnO-15 (N_2), (c) ZnO-30 (N_2), (d) ZnO-45 (N_2)

4. Conclusions

The variation of calcination temperature used does not change all ZnO crystal structures. However, increasing the calcination temperature can increase the crystallinity of the sample. It is known that low calcination temperature (150°C) has increased the crystallinity of ZnO by 13.5%. The degree of crystallinity increased from 49.9% (before calcination) to 80.6% (after calcination at 450°C in the N_2 environment). The TGA/DTA results show that the increase in crystallinity is related to the decomposition of components such as solvents and other compounds and the increasing number of crystals formed. Calcination temperature and air environment can affect the condition of natural defects (native defects) in ZnO compounds. Increasing the calcination temperature up to 450°C causes an increase in shallow traps related to interstitial zinc. The presence of a blueshift in the emission spectrum indicates this situation. The green emissions in samples calcinating at 150°C and 300°C (N_2) relate to deep traps related to oxygen vacancy defects. These results indicate that lower calcination temperatures lead to smaller crystal sizes, making them ideal for nano-optical applications like photocatalysis due to oxygen vacancies.

Acknowledgments

This work was supported by a Universitas Padjadjaran Research Grant (HRU-RPLK) fiscal year of 2023.

Bibliography

1. H. Morkoc, U. Özgür (2009). Zinc Oxide: Fundamentals, Materials and Device Technology. Weinheim: Wiley VCH.
2. N. Sharma, P.P Sahay (2023). Solution combustion synthesis of Dy-doped ZnO nanoparticles: An investigation of their structural, optical and photoluminescence characteristics,. Journal of Luminescence, 257. doi:10.1016/j.jlumin.2022.119655.
3. I. Ayoub, V. Kumar, R. Abolhassan, R. Sehgal, V. Sharma, R. Sehgal, Y. Mishra (2022). Advances in ZnO: Manipulation of defects for enhancing their technological potentials. Nanotechnology Reviews, 11(1). doi:10.1515/ntrev-2022-0035.
4. K.S. Siddiqi, A.U. Rahman, A. Husen (2018). Properties of Zinc Oxide Nanoparticles and Their Activity Against Microbes. Nanoscale Research Letters, 13(141). doi:10.1186/s11671-018-2532-3.
5. P. Porrawatkul, P. Nuengmatcha, A. Kuyyogsuy, R. Pimsen, P. Rattanaburi (2023). Effect of Na and Al doping on ZnO nanoparticles for potential application in sunscreens. Journal of Photochemistry and Photobiology B: Biology, 240, 1011-1344. doi:10.1016/j.jphotobiol.2023.112668.
6. S. Raha, M. Ahmaruzzaman (2022). ZnO nanostructured materials and their potential applications: progress, challenges and perspectives. Nanoscale Adv, 4(8), 1868-1925. doi:10.1039/D1NA00880C.
7. I. Islami (2023). Synthesis of ZnO-Al:TiO2 Materials and their Characterization as Photocatalyst Compounds. Applied Mechanics and Materials, Vol. 916, pp 71-80. doi: 10.4028/p-t9jofQ.
8. A. Anjum, R. Ahmed, Z.A. Umar, T. Hussain, M.N. Sarwar, M.A. Baig (2022). Structure and defects-related optical properties of highly (002)-oriented zinc oxide thin films. Physica B: Condensed Matter, 644. doi:10.1016/j.physb.2022.414195.

9. A. Moezzi, A.M. McDonagh, M.B. Cortie (2012). Zinc oxide particles: Synthesis, properties and applications. Chemical Engineering Journal, 185–186, 1-22. doi:10.1016/j.cej.2012.01.076.
10. A. Layek, S. Banerjee, B. Manna, A. Chowdhury (2016). Synthesis of rare-earth doped ZnO nanorods and their defect–dopant correlated enhanced visible-orange luminescence. RSC Adv, 6(42), 35892-35900. doi:10.1039/C6RA02278B.
11. Z.S. Shaymardanov, R.R. Rustamova, Z. Jalolov Sh, B.N. Urolov, B.N. Rustamova, R.R. Jalolov, S.Z. Urolov (2023). Influence of the nature of defects in ZnO nanocrystals synthesized by chemical bath deposition on photocatalytic activity. Physica B: Condensed Matter, 649. doi:10.1016/j.physb.2022.414444.
12. H. Shen, X. Shi, Z. Wang, Z. Hou, C. Xu, L. Duan, H. Wu (2022). Defects control and origins of blue and green emissions in sol-gel ZnO thin films. Vacuum, 202. doi:10.1016/j.vacuum.2022.111201.
13. M. Goswami, N.C. Adhikary, S. Bhattacharjee (2018). Effect of annealing temperatures on the structural and optical properties of zinc oxide nanoparticles prepared by chemical precipitation method. Optik, 158, 1006-1015. doi:10.1016/j.ijleo.2017.12.174.
14. D. Aryanti, E. Hastuti, M. Taspika et al. (2020). Characteristics and photocatalytic activityof highly c-axis-oriented ZnO thin films. Journal of Sol-Gel Science and Technology, 96(9). doi:10.1007/s10971-020-05361-5.
15. A.N. Rahmawati, N.P. Utami, L Safriani, A. Bahtiar, W.S. Arsyad, E.S. Nurazizah, A. Aprillia (2023). High Preferred Orientation on c-axis of ZnO: GO Crystal Film Synthesized Under Electric Field. Jurnal Penelitian Fisika dan Aplikasinya (JPFA), 13(2). doi:10.26740/jpfa.v13n2.p146-159.
16. M.U. Sumaya, K.H. Maria, F.Z. Toma et al. (2023). Effect of stabilizer content in different solvents on the synthesis of ZnO nanoparticles using the chemical precipitation method. Heliyon, 9(10).
17. R.N. Aljawvi, M.J. Alam, F. Rahman et al. (2018). Impact of annealing on the structural and optical properties of ZnO nanoparticles and tracing the formation of clusters via DFT calculation. Arabian Journal of Chemistry, 13(1). doi:10.1016/j.arabjc.2018.04.006.
18. L. Skowronski, A. Ciesielski, A. Olszewska, A. Szczesny, R. Naparty, M. Trzcinski, A. Bukaluk (2020). Microstructure and Optical Properties of E-Beam Evaporated Zinc Oxide Films—Effects of Decomposition and Surface Desorption. Materials, 13(16). doi:10.3390/ma1316351.
19. S. Simeonov, A. Szekeres, D. Spassov, M. Anastasescu, I. Stanculescu, M. Nicolescu, M. Gartner (2021). Investigation of the Effects of Rapid Thermal Annealing on the Electron Transport Mechanism in Nitrogen-Doped ZnO Thin Films Grown by RF Magnetron Sputtering. Nanomaterials, 12(1). doi:10.3390/nano1201001.
20. E.G. Goh, X. Xu, P.G. McCormick (2014). Effect of particle size on the UV absorbance of zinc oxide nanoparticles. Scripta Materialia, 78-79, 49-52. doi:10.1016/j.scriptamat.2014.01.033
21. P. L. Gareso, H. Heryanto, E. Juarlin, P. Taba (2023). Effectof Annealing onthe Structural and Optical Properties of ZnO/ITO and AZO/ITO Thin Films Prepared by Sol-Gel Spin Coating. Trends in Sciences, 20(3). doi:10.48048/tis.2023.6521.